Ab initio and embedded-atom-model simulation analysis of collective dynamics in liquid Fe at experimental high pressures

Taras Demchuk [1], Anatoly B. Belonoshko [2,3,4] and Taras Bryk [1,5,*]

[1] *Yukhnovskii Institute for Condensed Matter Physics of the National Academy of Sciences of Ukraine, 1 Svientsitskii Street, UA-79011 Lviv, Ukraine*

[2] *Frontiers Science Center for Critical Earth Material Cycling, School of Earth Sciences and Engineering, Nanjing University, Nanjing 210023, China*

[3] *Condensed Matter Theory, Department of Physics, AlbaNova University Center, Royal Institute of Technology (KTH), 10691 Stockholm, Sweden*

[4] *Department of Physics, University of South Florida, Tampa, Florida 33620, USA*

[5] *Institute of Applied Mathematics and Fundamental Sciences, Lviv Polytechnic National University, UA-79013 Lviv, Ukraine*

(Received 3 January 2025; revised 20 May 2026; accepted 7 August 2026; published 3 September 2026)

We compare extensive *ab initio* simulations and embedded-atom-model molecular dynamics for analysis of collective dynamics in liquid Fe at several experimental pressures and temperatures of 2200 and 2700 K [Y. Kuwayama *et al.*, Phys. Rev. Lett. **124**, 165701 (2020)]. Dynamic eigenmodes of the generalized Langevin equation were calculated based on simulation data and analyzed in a wide range of wave numbers with a focus on dispersion of collective excitations. We analyze the origin of positive dispersion of sound excitations in connection with contributions from different types of hydrodynamic and nonhydrodynamic fluctuations to the corresponding eigenvectors. Dispersion of collective excitations and adiabatic speed of sound, estimated from the simulation data at three pressures, is compared to the values obtained from the inelastic x-ray scattering experiments.

DOI: 10.1103/vzqb-lsq5

I. INTRODUCTION

Iron alloyed with about 10% Ni and light elements such as Si, S, C, H, O, and perhaps some others, is believed to be the major material composing the liquid (outer) core of the Earth [1–3]. The presence of Ni and its percentage in the outer core is evidenced by compositions of Fe-Ni meteorites, while the presence of light elements (with unknown content of of chemical elements) is required to match the density of the outer core. We know that liquid iron is denser than the outer core material at the same pressure and temperature. However, neither composition nor temperature in the outer core is known precisely. Most of the data on the outer core material come from sound waves propagating through the Earth's interior. By matching the properties of sound waves propagating through the core with the properties of various Fe alloys we get the information on the composition, density, temperature, and other properties of the material in the Earth's core. Experiments at the pressure (P)-temperature (T) conditions of the Earth's core (130–360 GPa and 3000–7000 K) are extremely difficult, technically. Many properties at extreme P and T have not yet even been measured, for example, density, speed of sound, viscosity, diffusivity, heat conductivity, heat capacity, sound wave attenuation, etc. Such data are critically needed to establish the models of Earth's formation and its evolution, to describe its past, present, and future. At the same time, theoretical methods have matured to the extent where we can trust the information they provide as much as we trust experimental data. Moreover, the physics behind the computed data and the level of detail provided by theoretical methods is superior to experiment. Recently, it was discovered that the outer core is not homogeneous as regards the direction of sound wave propagation [4]. This makes studies of the physics of sound propagation in liqiuds especially timely.

Various properties of iron in liquid and solid states were intensively studied in wide ranges of temperatures and pressures experimentally [5–10] and by computer simulations [11–27]. Recent x-ray diffraction and inelastic x-ray scattering (IXS) experiments on liquid Fe at high pressures [28] provided valuable information about the density and microscopic structure in the range of P and T from 21.5 GPa, 2600 K to 116.1 GPa, 4350 K and on the dynamic structure of pure molten Fe at three thermodynamic points (16.0 GPa, 2200 K), (32.7 GPa, 2700 K), and (44.9 GPa, 2700 K). The experimental dispersion curves $\omega(k)$ for collective excitations were reported in a range of wave numbers $0.3 - 0.57\,\text{Å}^{-1}$ and a linear extrapolation toward the macroscopic limit allowed one to estimate the macroscopic speed of sound in liquid Fe at those thermodynamic points.

On the side of computer simulations one can make use either of effective potentials for molecular dynamics (MD) simulations or explicitly treat the electron subsystem within

*Contact author: bryk@icmp.lviv.ua

Published by the American Physical Society under the terms of the Creative Commons Attribution 4.0 International license. Further distribution of this work must maintain attribution to the author(s) and the published article's title, journal citation, and DOI.

the density functional theory (DFT) in *ab initio* molecular dynamics (AIMD). The AIMD simulations are extremely time consuming for large simulated systems; therefore a robust effective potential for simulations of solid or liquid Fe is of great importance. One of the most successful types of effective potentials for iron is the embedded-atom-model (EAM) type potentials, like the one with parameters estimated from *ab initio* LMTO energy-volume dependence for hcp and liquid iron [14], where LMTO corresponds to a method of linear muffin-tin orbitals. Another robust well-known EAM potential for iron was suggested in [29]. Previous simulation studies of dynamic properties of liquid iron at high pressures were focused on calculations of transport coefficients [13,16,17,30] and estimation of sound speed [31], as well as phonon dispersion curves [18,32] and vibrational density of states [15,20] for solid iron. Collective dynamics and, in particular, dispersion of collective excitations in liquid Fe from simulations were studied for the states close to the melting line in [24–26] and at high pressures in [27].

Although the Curie temperature for iron is 1043 K and it is paramagnetic at higher temperatures on macroscopic scales, the local magnetic moments of ions cause spin polarization of the electron subsystem and contribute to the energetics and structure of solid and liquid Fe [33,34]. AIMD simulation studies [25,27,34] pointed out that local magnetic moments of ions and spin polarization should be taken into account for proper comparison with the experimental data on structure and dynamics. It was shown in [25] that the spin-polarized AIMD simulations result in more pronounced oscillations of the density-density time correlation functions, than those from nonmagnetic AIMD simulations.

It is not a simple task to estimate precisely the dispersion of collective excitations in liquids. In contrast to crystals or glasses, where the atoms are supposed to vibrate around the equilibrium positions, in liquids there are no stable local equilibrium positions for atoms because they take an active part in different relaxation processes: structural relaxation, diffusion, and heat transfer. The methodology of theoretical study of collective excitations in liquids must be based on generalized hydrodynamics. This permits one to study the viscous regime on macroscopic distances and elastic properties like in solids on meso- and microscopic spatial scales. There exist a few schemes of generalization of hydrodynamics [35–37]; however, for the purpose of calculations of dispersion of collective excitations from MD data, mainly a fit based on the memory function formalism [38–42] was applied. Another approach within mode coupling theory was suggested recently [43,44], having as an input only information on static structure factors $S(k)$. However heat fluctuations in this scheme are completely ignored which corresponds to viscoelastic description of liquids with the ratio of specific heats γ close to unity.

One of the most advanced methods of generalized hydrodynamics that was developed for the purpose of theoretical analysis of time correlation functions obtained in MD simulations is the approach of generalized collective modes (GCM) [45,46] which in fact corresponds to eigenomode calculations of the generalized Langevin equation. This theoretical approach is based on systematic extension of the set of hydrodynamic (conserved) variables by ones that are orthogonal to them, that are supposed to describe correctly more short-time collective processes in comparison with most slow hydrodynamic ones. The extended set of N dynamic variables is then used for calculation of a $N \times N$ generalized hydrodynamic matrix $\mathbf{T}(k)$ for each wave number k, eigenvalues of which correspond to either relaxing (real eigenvalues) or propagating (pairs of complex-conjugated eigenvalues) modes that can exist in the system. Since the hydrodynamic set of dynamic variables contains energy (or heat) density the GCM approach is able to reproduce correctly all the features of crossover between leading thermal relaxation in the long-wavelength region and structural relaxation on the boundary of the hydrodynamic regime as well as the so-called "positive dispersion" of acoustic excitations that is connected with this crossover [47]. Our aim is to apply the GCM methodology to the simulation data obtained from EAM and *ab initio* simulations of liquid Fe at the three thermodynamic points studied by the IXS experiments, and another point at the lowest pressure of 16 GPa and temperature 2700 K. We will study the dispersion of collective excitations as the eigenmodes of the generalized Langevin equation, and analyze the behavior of components of the eigenvectors corresponding to the acoustic eigenvalues. Another aim is to estimate the macroscopic adiabatic speed of sound at different thermodynamic points based on recently suggested methodology [48] and to compare these values to the IXS experimental results [28].

The generalized hydrodynamics of liquids with local magnetic moments was not elaborated on the level of the GCM methodology to be used in analysis of time correlation functions, obtained from the spin-polarized AIMD simulations. We would like to mention the hydrodynamic description of magnetic liquids developed in [49] and expressions for hydrodynamic modes and hydrodynamic time correlation functions of the liquids with Heisenberg spin-spin interaction [50,51]. It was shown that, in addition to the standard three hydrodynamic longitudinal modes in one-component nonmagnetic liquids (two propagating sound modes and one thermal relaxing mode), there exists another magnetic diffusive mode, which causes an additional damping of the propagating acoustic excitations [51]. However, by this date there is no generalized hydrodynamic theory of magnetic liquids that is able to shed light on possible nonhydrodynamic collective modes as this is for nonmagnetic liquids. The hydrodynamic approach developed for isotropic magnetic liquids cannot be directly applied to the analysis of collective dynamics observed in spin-polarized AIMD simulations of rather small simulated systems, i.e., for typical wave numbers outside the hydrodynamic regime. Furthermore, the generalized hydrodynamic approach has to account for "magnetic" density $n_m(k)$ at different spatial scales, which should differ from the regular density of particles $n(k)$ because of the spin polarization of the electron subsystem. This causes a need to include in numerical generalized hydrodynamic analysis two components of spin-polarized electron density, which in their turn usually are calculated in spin-polarized AIMD in adiabatic approximation. Hence there are many unclear issues of how to construct a working scheme of analysis of time-dependent density-density correlations obtained from spin-polarized AIMD simulations. Therefore in the actual study we restricted ourselves by considering only the nonmagnetic state of liquid Fe in AIMD; however, we performed it

for the most advanced analysis of hydrodynamic and nonhydrodynamic modes in the collective dynamics of nonmagnetic EAM and AIMD simulations.

The remaining part of the paper has the following structure. In the next section we provide information about the computer simulations of liquid Fe and details of the GCM analysis of the simulation data. Section III contains the results of this study and corresponding discussion. The last section contains the conclusions of this study.

II. SIMULATIONS AND ANALYSIS OF SIMULATION DATA

We performed MD simulations with EAM potentials for liquid Fe at two temperatures, 2200 and 2700 K, and for temperature 2700 K we considered three pressures. Three of the simulated conditions corresponded to thermodynamic points studied in the IXS experiments [28]. The simulated system was composed of 16 000 particles in a periodic cubic box, the size of which corresponded to desired pressures. The EAM interactions for liquid iron were taken from Ref. [29]. The simulations of production runs in equilibrated systems were performed over the 80 000 time steps ($\delta t = 1$ fs) with sampling at each second step for each thermodynamic point. The system was equilibrated in the *NVT* ensemble using the Nosé-Hoover chain of thermostates, while the *NVE* ensemble was used for a production run. The smallest wave numbers in these simulations were between $k_{\min} = 0.1096$ Å^{-1} (at the lowest pressure of 16 GPa and $T = 2700$ K) and 0.1156 Å^{-1} (at the highest pressure of 44.9 GPa and $T = 2700$ K).

Ab initio simulations of liquid Fe at $T = 2700$ *K* and pressure $P = 45$ GPa were performed using a system of 1000 particles with electron-ion interaction as projector-augmented-wave (PAW) potentials [52,53] with 16 valence electrons. The exchange-correlation functional was taken in the generalized gradient approximation using a Perdew-Burke-Ernzerhof (GGA-PBE) form [54]. The plane-wave expansion of wave functions had a cutoff energy of 400 eV, and for electron density we took just a single Γ point of the Brillouin zone. The box length at the reference pressure was 21.2677 Å, that allowed one to reach the smallest wave number $k_{\min} = 0.295$ Å^{-1}.

For analysis of collective dynamics we applied a generalized collective mode (GCM) methodology [45,55], which is based on recovering the simulation-derived time correlation functions by GCM eigenmodes and associated eigenvectors [45]. For the need of calculations of time correlation functions and their GCM analysis we sampled from MD data the following Fourier components of microscopic hydrodynamic variables: density of particles,

$$n(k,t) = \frac{1}{\sqrt{N}} \sum_{i=1}^{N} e^{-i\mathbf{k}\mathbf{r}_i}, \tag{1}$$

and density of longitudinal $J^L(k,t)$ and transverse $J^T(k,t)$ mass currents,

$$J^{L/T}(k,t) = \frac{m}{\sqrt{N}} \sum_{i=1}^{N} v_i^{L/T} e^{-i\mathbf{k}\mathbf{r}_i}, \tag{2}$$

where $v_i^{L/T}(t)$ are the longitudinal and transverse projections of the ith particle velocity with respect to the direction of the **k** vector. The Fourier components of energy density were expressed as

$$e(k,t) = \frac{1}{\sqrt{N}} \sum_{i=1}^{N} \varepsilon_i e^{-i\mathbf{k}\mathbf{r}_i}, \tag{3}$$

with the single-particle energies calculated according to the EAM model,

$$\varepsilon_i = \frac{1}{2} m v_i^2 + \frac{1}{2} \sum_{j \neq i}^{N} \Phi(r_{ij}) + F(\rho_{el}), \tag{4}$$

with $\Phi(r)$ being the pairwise interaction between two atoms and $F(\rho)$, the embedding function, which depends on local electron density.

For the GCM analysis of collective dynamics in one-component liquids, which is based on the matrix form of the generalized Langevin equation, we made use of the thermoviscoelastic (TVE) set of five dynamic variables used to construct the corresponding matrices,

$$\mathbf{A}^{(5)}(k,t) = \{n(k,t), J^L(k,t), h(k,t), \dot{J}^L(k,t), \dot{h}(k,t)\}. \tag{5}$$

Here the dynamic variable of heat density $h(k,t)$ is defined as follows,

$$h(k,t) = e(k,t) - \frac{\langle n(-k,0) e(k,0)\rangle}{\langle n(-k,0) n(k,0)\rangle} n(k,t), \tag{6}$$

and the overdots in (5) mean the first time derivative of (2) and of $h(k,t)$ according to the expressions (1), (3), and (6). These extended (nonhydrodynamic) variables are straightforward to calculate from the MD trajectories and velocities of particles. Note that the thermoviscoelastic set of dynamic variables within the GCM methodology provides exact recovering by TVE theory of the first five frequency moments of MD-derived dynamic structure factor $S(k,\omega)$, as well as the lowest time moment of the density-density time correlation function which is equal to the value $S(k,\omega=0)$. The highest fourth frequency moment of $S(k,\omega)$, recovered in this five-variable GCM approach, is directly related to the second frequency moment of the longitudinal current spectral function $C^L(k,\omega)$ [35,36]. The latter is easily obtained from simulations via static current correlators as

$$\langle \omega_L^2(k)\rangle = \frac{\langle \dot{J}^L(-k,0)\dot{J}^L(k,0)\rangle}{\langle J^L(-k,0)J^L(k,0)\rangle} = c_\infty^2(k)k^2, \tag{7}$$

and allows one to make a direct definition of the high-frequency k-dependent speed of sound $c_\infty(k)$ and its macroscopic ($k \to 0$) value c_∞, because one easily recovers the k^2 dependence of $< \omega_L^2(k) >$ in the long-wavelength region from MD simulations. In its turn this leads to the estimation of the macroscopic adiabatic speed of sound c_s [48] via

$$c_s = \sqrt{c_\infty^2 - \psi^L(0)/\rho}, \tag{8}$$

where

$$\psi^L(0) = \frac{V}{k_B T} \langle (\sigma_{zz}(0) - \bar{P})(\sigma_{zz}(0) - \bar{P})\rangle,$$

with $\bar{P}$ being the average pressure over the production run and $\sigma_{zz}(t=0)$ the diagonal components of the stress tensor; ρ is the mass density.

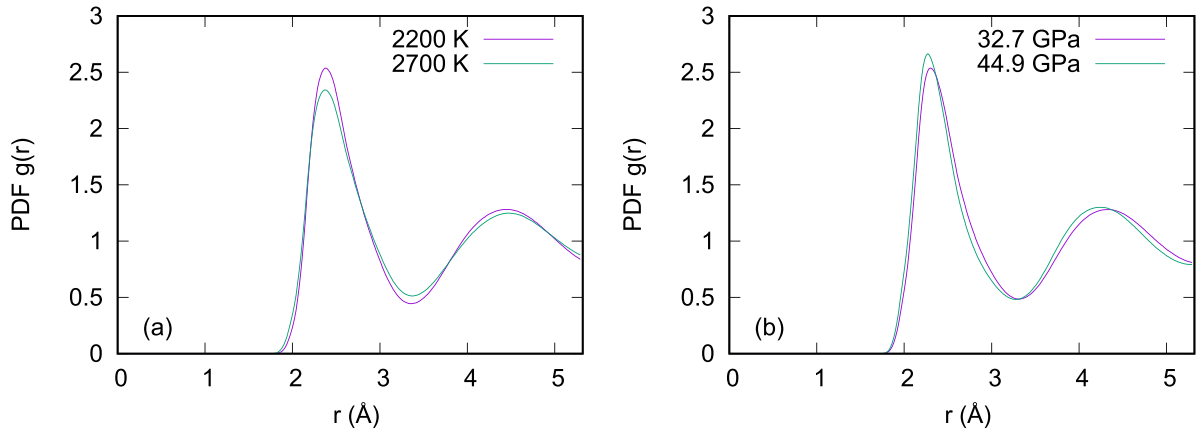


FIG. 1. Pair distribution functions for liquid iron at pressure 16 GPa and temperatures 2200 and 2700 K (a) and at pressures 32.7 and 44.9 GPa and temperature 2700 K (b).

The thermoviscoelastic set of dynamic variables was used for estimation of the 5×5 generalized hydrodynamic matrix $\mathbf{T}(k)$ via

$$\mathbf{T}(k) = \mathbf{F}(k, t = 0)\tilde{\mathbf{F}}^{-1}(k, z = 0), \tag{9}$$

where the matrix elements of 5×5 matrices of static correlation functions $\mathbf{F}(k, t = 0)$ and of Laplace-transformed time correlation functions in Markovian approximation $\tilde{\mathbf{F}}(k, z = 0)$ can be obtained directly from MD simulations. The eigenvalues of the generalized hydrodynamic matrix $\mathbf{T}(k)$ (real or pairs of complex-conjugated ones) correspond to relaxing or propagating collective modes existing in the studied system, while corresponding eigenvectors allow one to estimate the origin of each dynamic eigenmode and its contribution to the time correlation functions of interest. The GCM methodology allows one to express the time correlation functions via dynamic eigenmodes of the TVE dynamic model as

$$F_{ij}^{(5)}(k, t) = \sum_{\alpha=1}^{5} G_{ij}^{\alpha}(k) e^{-z_{\alpha}(k)t}, \quad i, j = \mathbf{A}^{(5)}, \tag{10}$$

where the generally complex amplitudes of contributions from five dynamic eigenmodes $G_{ij}^{\alpha}(k)$ are expressed via the corresponding eigenvectors [45]:

$$G_{ij}^{\alpha}(k) = \sum_{l=1}^{5} X_{i,\alpha} X_{\alpha,l}^{-1} F_{lj}(k, t = 0). \tag{11}$$

Here the matrix $X_{i,\alpha}(k)$ has each α-th column composed of components of the associated eigenvector with the α eigenvalue $z_{\alpha}(k)$, which are complex numbers in general. One of the main aims of this study is to focus on the wave-number dependence of the components of eigenvectors associated with sound eigenvalues in order to rationalize the origin of acousticlike modes in different k regions.

For the case of *ab initio* simulations the fit-free analysis of collective dynamics in liquid metals faces essential problems because of complications with direct sampling of dynamic variables $h(k, t)$ and $\dot{h}(k, t)$ in the thermoviscoelastic set of five dynamic variables (5) from AIMD. Here we will make use of the TVE analysis from AIMD simulations proposed in [56], which contains some fitting parameters; however, it is based on the same expressions for mode contributions and GCM time correlation functions (10).

III. RESULTS AND DISCUSSION

A. Embedded-atom-model simulations

Pair distribution functions $g(r)$ of liquid Fe at the four studied thermodynamic points are shown in Fig. 1. The general well-known tendency is observed in behavior of the $g(r)$ in dependence on temperature and pressure. In the absence of specific structural transformations in the metallic Fe melt we observe a small shift of the $g(r)$ and, in particular, the first maximum of $g(r)$ with pressure toward smaller distances. At $T = 2700$ K the increase of pressure results in a shift of the first maximum of $g(r)$ from 2.37 Å at $P = 16$ GPa to 2.26 Å at $P = 44.5$ GPa and an increase of the number of nearest neighbors in the first coordination shell from 13.1 to 14.94, respectively. At the fixed pressure (16 GPa) the effect of temperature decrease is mainly in making the oscillations of the $g(r)$ more pronounced; in particular, it is seen in the increase of the amplitude of the first maximum of $g(r)$ and

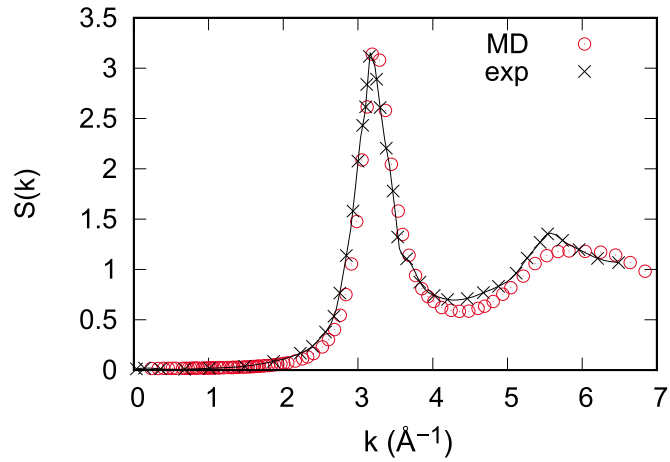


FIG. 2. Static structure factor from MD simulations at pressure 44.9 GPa and temperature 2700 K in comparison with available x-ray diffraction data at $T = 2700$ K and $P = 42$ GPa [28].

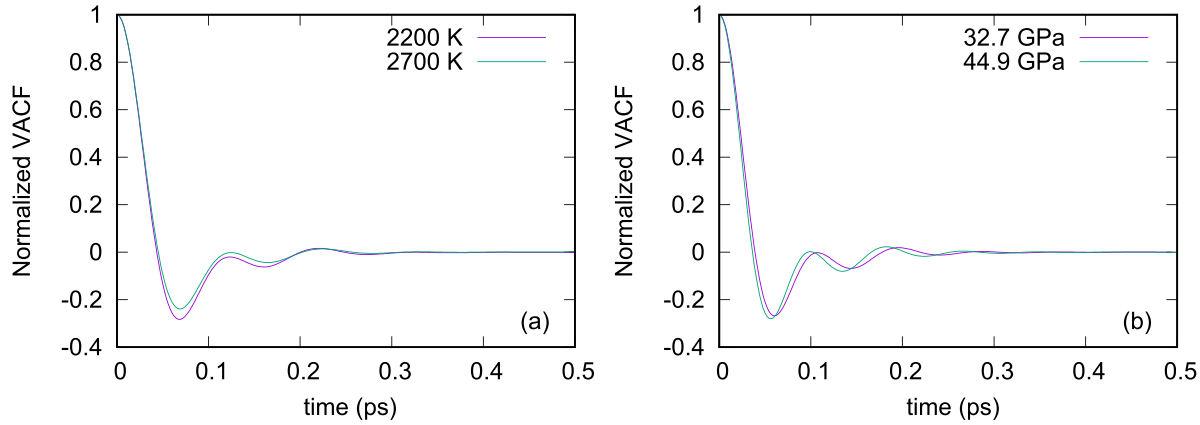


FIG. 3. Normalized velocity autocorrelation functions for liquid Fe at 16 GPa (a) and two higher pressures at $T = 2700$ K (b).

decrease of the value at the first minimum of $g(r)$, while the first maximum and minimum remain practically at the same distance of 2.37 and 3.34 Å, respectively. The number of nearest neighbors slightly decreases with temperature at the fixed pressure of 16 GPa, from 13.3 at $T = 2200$ K to 13.1 at $T = 2700$ K.

The Fourier transform of spherically symmetric pair correlation function $g(r) - 1$ is directly related to the static structure factor $S(k)$, while for estimation of $S(k)$ from our simulations we made use of another definition of $S(k)$ as the instantaneous density-density correlation function, which is the value of the density-density time correlation function $F_{nn}(k, t)$ at origin

$$S(k) \equiv F_{nn}(k, t = 0) = \langle n_{-k} n_k \rangle. \tag{12}$$

Note that this method of estimation of the $S(k)$ as well as of the density-density time correlation functions $F_{nn}(k, t)$ from simulations requires an additional average over all possible directions of k-vectors having the same absolute value (spherical average). In Fig. 2 we show how the calculated static structure factor $S(k)$ for liquid Fe at temperature 2700 K and pressure 44.9 GPa corresponds to the experimental data (which was available for the closest pressure of 42 GPa in x-ray diffraction experiments reported in [28]. One can see a reasonable agreement with the experimental $S(k)$ despite a difference in simulation and experimental pressures.

Single-particle dynamics is usually represented by the velocity autocorrelation functions (VACFs), which, for the four studied thermodynamic points, are shown in Fig. 3. At all four states the VACFs show typical behavior as for dense liquids having in their time dependence a well-defined negative region, which corresponds to backscattering of particles on the nearest neighbors and is known as the "cage effect." A comparison between the four states from the point of view of single-particle dynamics is better to perform in frequency domain. Therefore we show in Fig. 4 the power spectra of VACFs, which outside the low-frequency region correspond to the vibrational density of states (VDOS). At a lower pressure of 16 GPa we see that both spectra in Fig. 4(a) show a well-defined maximum at $\sim 28\,\mathrm{ps}^{-1}$ and a high-frequency shoulder, while at $T = 2700$ K [Fig. 4(b)] the increase of pressure leads to a shift of the shoulder toward higher pressures and transformation into a pronounced second maximum at $\sim 62\,\mathrm{ps}^{-1}$. This information is important in the next analysis of the dispersion curves in order to estimate the excitations responsible for maxima in VDOS.

The collective dynamics of liquid Fe at all four thermodynamic points were analyzed by the fit-free GCM methodology within the thermoviscoelastic dynamic model (5), i.e., with correct treatment of hydrodynamic thermal relaxation and nonhydrodynamic thermal processes described by the presence of the heat density and its first time derivative in the

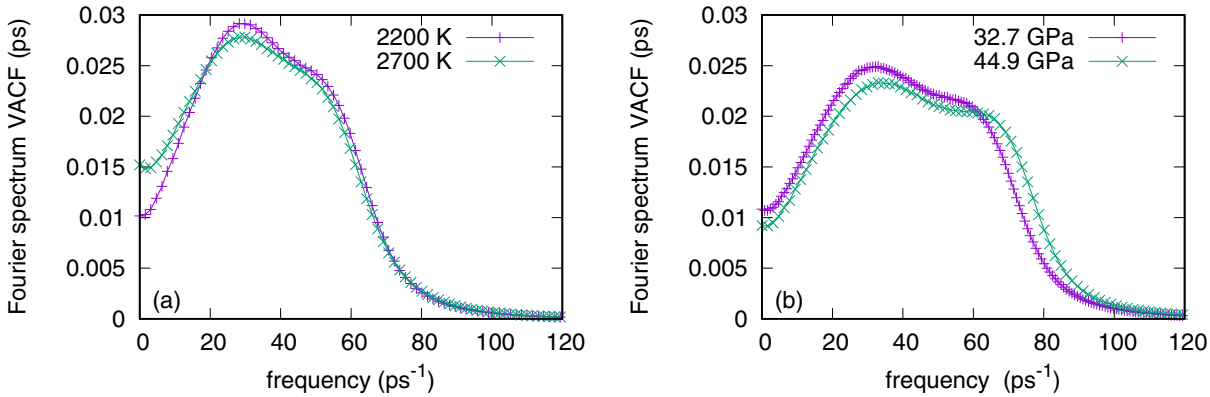


FIG. 4. Fourier spectra of the four velocity autocorrelation functions: at 16 GPa (a) and two higher pressures at $T = 2700$ K (b). Outside the low-frequency region the Fourier spectrum is proportional to the vibrational density of states.

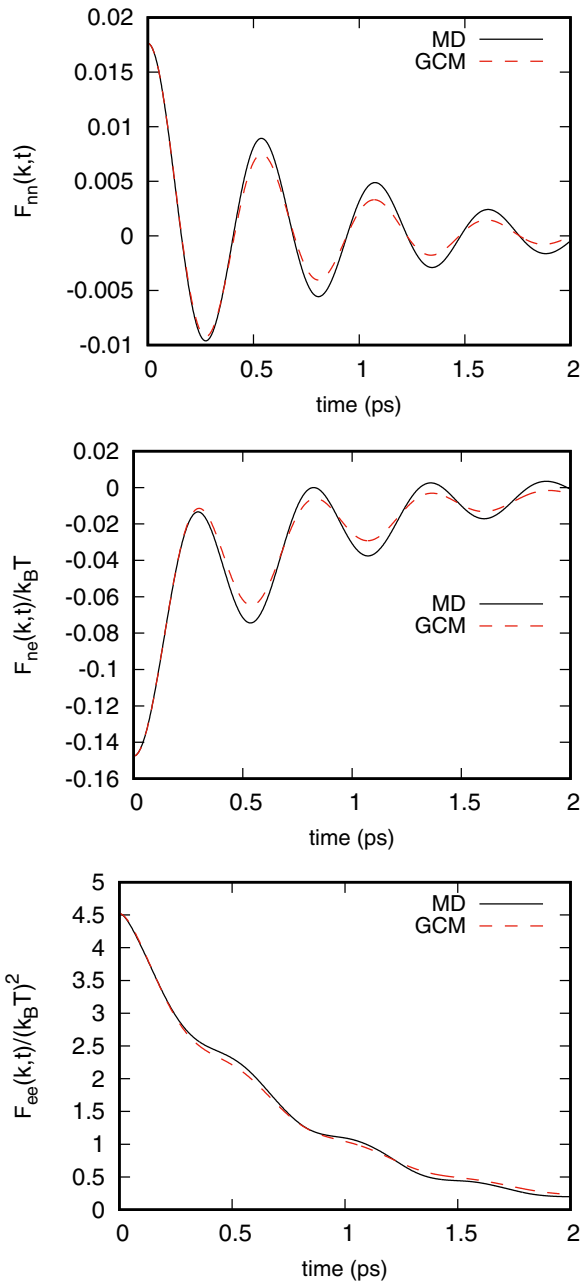


FIG. 5. Fit-free recovering of MD-derived density-density, density-energy, and energy-energy time correlation functions (solid line) by GCM dynamic eigenmodes at $k = 0.160\,\text{Å}^{-1}$ for liquid iron at $T = 2700$ K and $P = 32.7$ GPa.

set of five interacting dynamic variables. The quality of the GCM theory is seen from Fig. 5, where the MD-derived three time correlation functions (density-density, density-energy, and energy-energy) are very nicely recovered by the theoretical GCM expression based on calculated eigenmodes $z_\alpha(k)$ and corresponding contributions from these eigenmodes to the time correlation functions (10).

The dispersion of the propagating eigenmodes of liquid Fe at $P = 16$ GPa and temperature 2200 K is shown in Fig. 6. Two branches of collective excitations (propagating modes) correspond to the acoustic branch (open circles) and nonhydrodynamic heat waves (open triangles). The effect of thermal fluctuations and heat waves (representing the wave-like mechanism of heat transfer) on sound excitations will be seen later, when we analyze the k dependence of components of sound eigenvectors. Here we have to stress that similarly to the shear waves (transverse excitations) the heat waves have a so-called propagation gap in the long-wavelength region [46], which means they are absent at macroscopic distances and exist only on nanoscales. At $k_H < 0.6\,\text{Å}^{-1}$ the hydrodynamic heat relaxation plays a main role in bringing the spatially remote regions with different local temperature to thermal equilibrium, while on distances smaller than $2\pi/k_H$ the heat waves took part in this equilibration too. The dispersion of acoustic modes shows a deviation from linear law $\omega \sim k$ in the long-wavelength region toward higher frequencies known as a "positive dispersion." This effect is very clearly seen in the right frame of Fig. 6. In general, good agreement with the IXS experimental data (shown by red cross symbols) is observed, although our smallest available wave number allowed us to estimate a little smaller apparent speed than in the case of IXS experiments.

One can observe similar behavior of dispersion of collective propagating eigenmodes (acoustic modes and heat waves) in the case of two other thermodynamic points at $P = 32.7$ GPa at $T = 2700$ K (shown in Fig. 7) and $P = 44.9$ GPa at the same temperature (shown in Fig. 8). In both cases there is a bit lower frequency for the sound excitations at the smallest available wave number from our simulations than the estimated experimental IXS sound dispersion, although in general the agreement is reasonable as it is seen from the left frames in Figs. 7 and 8. The values of the high-frequency speed of sound c_∞ and adiabatic speed of sound c_s estimated from Eq. (8) and IXS experimental values reported in [28] are shown in Table 1.

We show in Fig. 9 that the high-frequency speed of sound c_∞ can be estimated very precisely from the long-wavelength asymptote of $\langle\omega_L^2(k)\rangle$ according to Eq. (7). This value is then used together with the instantaneous stress-stress correlations in the estimation of the macroscopic adiabatic speed of sound c_s according to Eq. (8). We show in Fig. 10 how well the macroscopic adiabatic speed of sound c_s at $P = 49.9$ GPa (solid line) calculated in this way corresponds to the apparent speed of sound eigenvalues $c_{\text{app}}(k) = \text{Im}[z_{\text{sound}}(k)]/k$ and to the another methodology of estimation of the adiabatic speed of sound via the extrapolation [46],

$$c_s^2 = \frac{k_B T}{m} \lim_{k\to 0} \frac{\gamma(k)}{S(k)}, \tag{13}$$

TABLE I. Thermodynamic points studied in EAM simulations and estimated values of the high-frequency c_∞ and adiabatic c_s speeds of sound. The experimental values of the adiabatic speed of sound c_{exp} were taken from Ref. [28].

P (GPa)	T (K)	c_∞ (m/s)	c_s (m/s)	c_{exp} (m/s)
16.0	2200	5674.5	4393.6	5030
16.0	2700	5612.5	4317.7	—
32.7	2700	6174.9	4837.9	5400
44.9	2700	6496.2	5220.4	5820

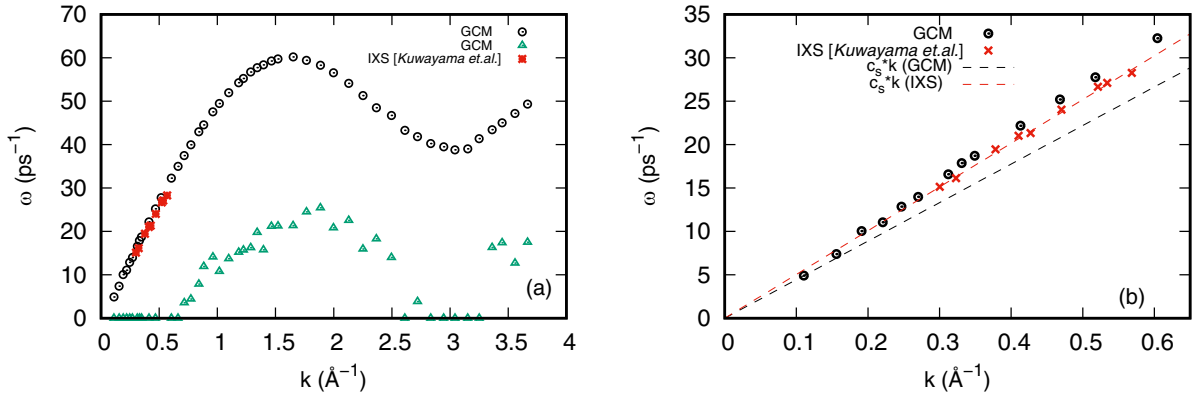


FIG. 6. Dispersion of longitudinal collective propagating modes at $T = 2200$ K and $P = 16.0$ GPa (a) and low-k region of the acoustic branch (b) in comparison with IXS experiments (red crosses). Triangle symbols in (a) correspond to dispersion of nonhydrodynamic low-frequency heat waves, which contribute to the heat transfer on nanoscales.

where $S(k)$ is the structure factor and $\gamma(k)$ is the k-dependent ratio of specific heats, which is directly expressed via static correlators we used in the GCM approach [45,55]. One can see that the apparent speed of sound shows the "positive dispersion" of 18% and which tends in the $k \to 0$ limit to the macroscopic value c_s estimated by Eq. (8), as well as to the other methodology (13). In agreement with Fig. 8 the experimental values of the apparent speed of sound have slightly higher values.

In order to rationalize the origin of the extended acoustic excitations in a wide range of wave numbers we estimated the k-dependent components of corresponding eigenvectors. In Fig. 11 we show the absolute value (because they are complex numbers in general) of each component $|X_i$, sound$|(k)$ with index "i" corresponding to the orthogonalized dynamic variable in the five-variable thermoviscoelastic set (5). Several important conclusions can be made from analysis of the k-dependent contributions to the eigenvectors of the sound excitations: (i) on macroscopic distances (in the long-wavelength limit) the sound excitations propagate solely due to the coupling of density and longitudinal current fluctuations, while a relatively small contribution from heat fluctuations is coming from the difference of local temperatures of densified and rarefied regions of the wave during the adiabatic propagation and is responsible for the increase of the propagation speed from isothermal to adiabatic value; (ii) there exists a crossover between the macroscopic mechanism of sound propagation due to conservation laws and elastic mechanism like in solids; (iii) the main crossover in contributions to the mechanism of sound propagation on different length scales is between density and stress tensor fluctuations, which implies the increase of the contribution from instantaneous microscopic forces between particles to the propagation of sound on nanoscales and obviously reflects the increase of elasticity in the viscoelastic transition in sound propagation; (iv) the rapid increase of contribution from the stress tensor in the region up to 0.5 Å^{-1} is responsible for the "positive sound dispersion" observed in this region of wave numbers for apparent speed of sound (Fig. 8) and is in agreement with the theory of positive sound dispersion reported in [47]; (v) in the region of wave numbers $1 - 3$ Å^{-1} the heat fluctuations do not play a significant role in the sound propagation, which explains why viscoelastic theories were successful in recovering the collective dynamics of liquids outside the hydrodynamic regime. These conclusions are very important from the point of view of understanding the viscoelastic transition and in particular the origin of positive sound dispersion in liquids. Note that the k-dependent components of eigenvectors in Fig. 11 and

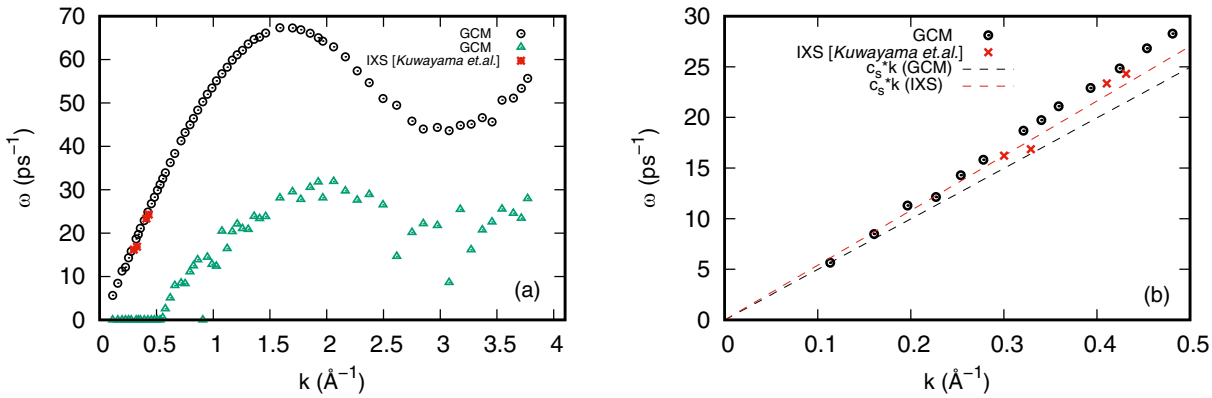


FIG. 7. Dispersion of longitudinal collective propagating modes at $T = 2700$ K and $P = 32.7$ GPa (a) and low-k region of the acoustic branch (b) in comparison with IXS experiments. Symbol correspondence as in previous figure.

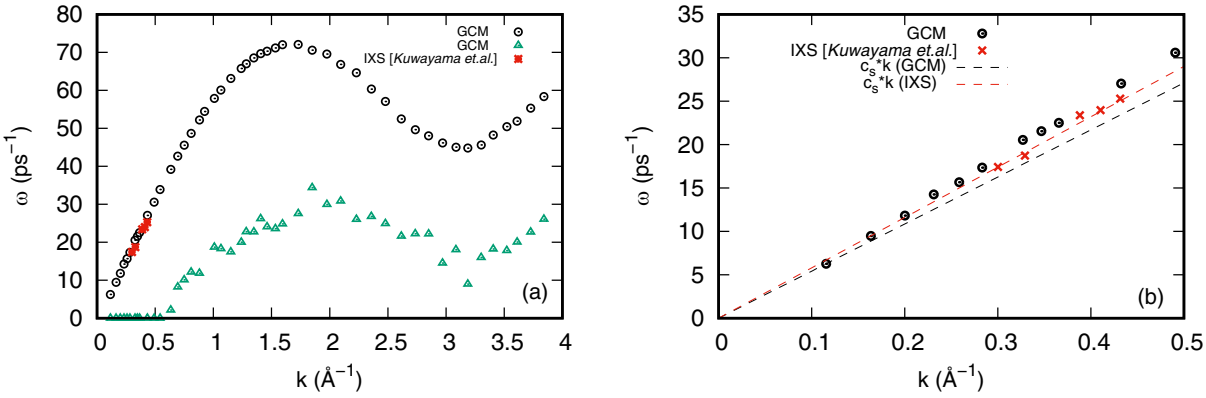


FIG. 8. Dispersion of longitudinal collective propagating modes at $T = 2700$ K and $P = 44.9$ GPa (a) and low-k region of the acoustic branch (b) in comparison with IXS experiments. Symbol correspondence as in previous figure.

analysis of the sound origin at different spatial scales as is shown here is a new feature of the GCM analysis of collective dynamics.

B. *Ab initio* simulations

Ab initio simulations of liquid Fe at $P = 45$ GPa and temperature 2700 K allow one to explicitly treat the electron subsystem in modeling within the density functional theory (DFT). Such *ab initio* approach is preferable at high pressures when the distribution of electron density can be essentially nonuniform, which can be responsible for specific short-range structure of liquid metals that is reflected on dynamic properties [57,58].

In Fig. 12 we compare pair distribution functions of the Fe particles obtained from EAM and *ab initio* simulations at the same *P-T* conditions. As one can see from Fig. 12 there is some small difference in behavior of $g(r)$ from two simulations. The softness of the core they describe varies similarly as one can judge from the behavior of $g(r)$ up almost to the first maximum. One can expect that there should be a difference in dynamics as well.

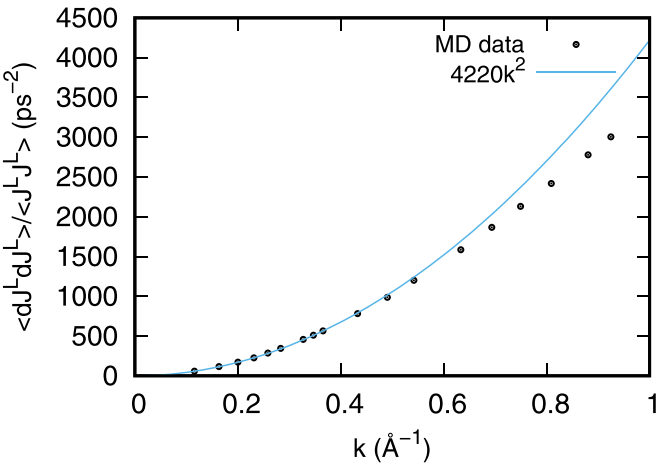


FIG. 9. Normalized second frequency moment of the longitudinal current spectral function (7) with $c_\infty^2 k^2$ asymptote in the long-wavelength limit used for estimation of the macroscopic adiabatic speed of sound for liquid iron at $T = 2700$ K and $P = 44.9$ GPa.

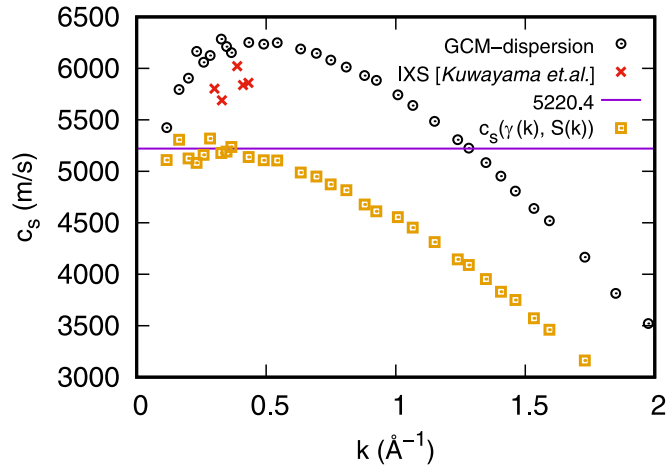


FIG. 10. Apparent speed of sound $\omega(k)/k$ with the estimated c_s via Eq. (8) in comparison with experimental IXS values of the apparent speed of sound (red cross symbols). Open boxes correspond to another methodology of estimation of c_s via the long-wavelength asymptote of $\gamma(k)/S(k)$ [48].

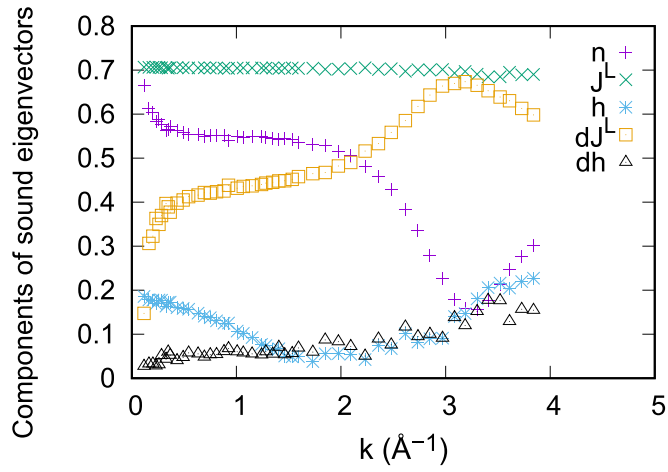


FIG. 11. Absolute values of k-dependent components of eigenvectors corresponding to propagating acousticlike excitations (eigenmodes with dispersion law shown in Fig. 8 by open circles). Contributions from different types of fluctuations are labeled according to the thermoviscoelastic dynamic model (5).

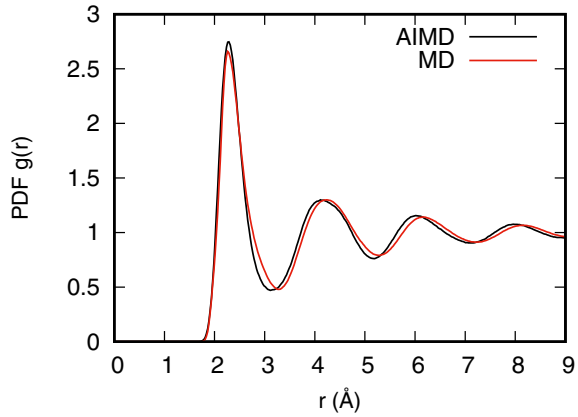


FIG. 12. Pair distribution functions for liquid iron from EAM and *ab initio* simulations at pressure 45 GPa and temperature 2700 K.

Indeed, the velocity autocorrelation functions shown in Fig. 13 have more pronounced oscillating behavior from *ab initio* simulations that is reflected in two well-resolved maxima at $\sim$38 and $\sim$66 ps^{-1} in the shape of the VACF Fourier spectrum. In comparison with the EAM simulations the maxima of the Fourier spectrum (practically VDOS) got shifted toward higher frequencies. The Fourier spectrum at zero frequency is directly related to the diffusion constant, which means the *ab initio* simulations resulted in about 30% smaller diffusivity than in the EAM simulations at the same thermodynamic point.

An important insight in collective dynamics can be obtained from the Van Hove time correlation function $G(r,t)$ [59,60], which is the time-dependent version of the pair correlation function and permits analysis of dynamics in real space. When Fourier transformed to momentum space it is exactly the density-density time correlation function $F_{nn}(k,t)$. In Fig. 14 we show the Van Hove time correlation functions for liquid Fe at 2700 K as obtained from EAM [Fig. 14(a)] and AIMD [Fig. 14(b)] simulations. At $t=0$ the $G(r,t)$, which consists of self- and distinct-particle contributions, is simply the pair correlation function. With increasing time the self-contribution to $G(r,t)$ develops the contribution at small distances due to displacements of particles from initial positions, while the distinct-particle contribution to $G(r,t)$ is responsible for time decay of the first, second, and other coordination shells. From comparison of $G(r,t)$ obtained from EAM and AIMD simulations one can say that the structure of liquid Fe in AIMD simulations is more rigid because the correlations in the initial coordination shells last for longer time than those in EAM simulations of our liquid Fe system.

To perform the GCM analysis of collective dynamics in the case of *ab initio* simulations one faces a problem of sampling directly from simulations the dynamic variable of energy $e(k,t)$ or heat density $h(k,t)$ within DFT and their first time derivatives. To avoid this problem we made use of the GCM methodology suggested in [56], namely, for GCM applications with *ab initio* simulations of pure liquids, which was recently extended to binary melts [61]. In Fig. 15 we show how the five-variable thermoviscoelastic model recovers the AIMD-derived density-density and longitudinal current-current time correlation functions in a wide range of wave numbers.

In Fig. 16 we compare the dispersion of acoustic eigenmodes obtained from GCM analysis of collective dynamics from *ab initio* and EAM simulations of liquid Fe at pressure 45 GPa and temperature 2700 K. In line with smaller diffusivity observed in *ab initio* simulations we observe slightly higher frequencies of the acoustic modes (which implies more rigid elastic properties of the liquid system) than in the EAM simulations. In general, the agreement with experimental dispersion obtained from IXS [28] and shown in Fig. 16 by red cross symbols is much better with the EAM simulation data. Note that the EAM and AIMD simulations performed at the reference pressure of IXS experiments 45 GPa had slightly different density of particles.

IV. CONCLUSIONS

We reported the theoretical analysis of collective dynamics of liquid Fe at IXS experimental pressures 16, 32.7, and 44.9 GPa and two temperatures, 2200 and 2700 K. The theoretical analysis was based on a combination of computer simulations and the GCM approach for estimation of dynamic eigenmodes of the generalized Langevin equation. The EAM and *ab initio* simulations were used to estimate the matrix elements of the 5×5 generalized hydrodynamic matrix $\mathbf{T}(k)$ that corresponded to the thermoviscoelastic dynamic model,

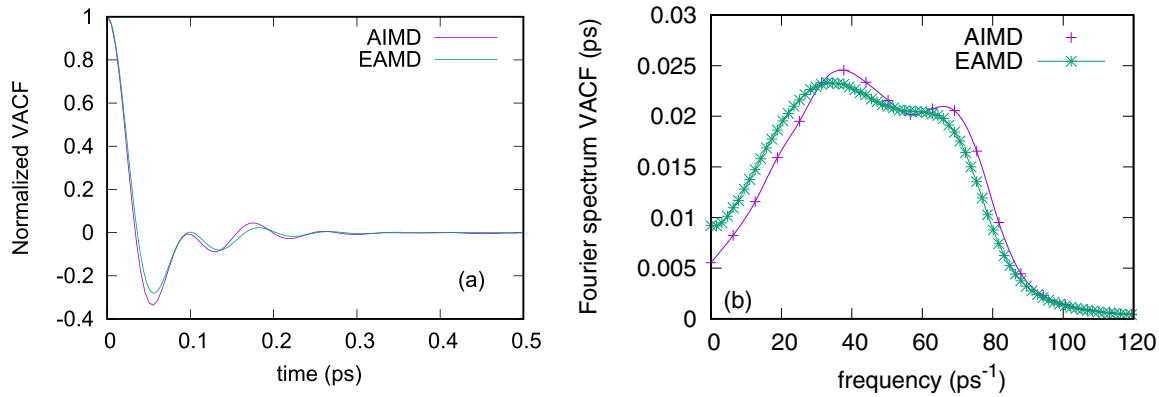


FIG. 13. Normalized velocity autocorrelation functions for liquid iron from EAM and *ab initio* simulations at pressure 45 GPa and temperature 2700 K (a) and their Fourier spectra (b).

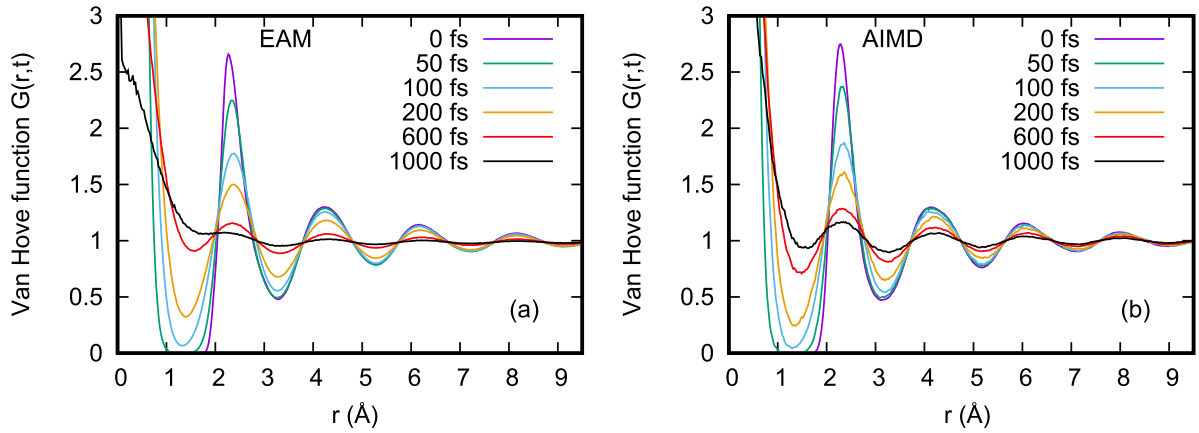


FIG. 14. Van Hove density-density time correlation functions $G(r, t)$ in liquid iron from EAM (a) and *ab initio* simulations (b) at pressure 45 GPa and temperatures 2700 K.

while the calculations of eigenvalues of $\mathbf{T}(k)$ for each k point sampled in simulations, and corresponding eigenvectors allowed one to estimate dispersion of collective excitations and mechanisms of sound propagation at different spatial scales in liquid Fe.

The main results of this study are the following:

(i) We found that the EAM potentials [29] allow quite good recovery of the experimental dispersion of collective excitations reported from IXS experiments at three high pressures and two temperatures [28]. We were able in our EAM simulations to reach smaller wave numbers than the lowest available from IXS experiments in Ref. [28], which allowed us to correct the estimated adiabatic speed of sound at those experimental thermodynamic points.

(ii) The *ab initio* simulations performed with 1000 Fe atoms in GGA-PBE at $P = 45$ GPa resulted in dispersion of collective excitations with slightly higher frequencies than the experimental ones and those obtained from EAM simulations. A comparative analysis of pair distribution functions, velocity autocorrelations, Van Hove time correlation functions, and dispersion of collective excitations from EAM and AIMD simulations for liquid Fe at $T = 2700$ K are evidence that the AIMD simulations with GGA-PBE correspond to a more rigid system with overestimated frequencies in

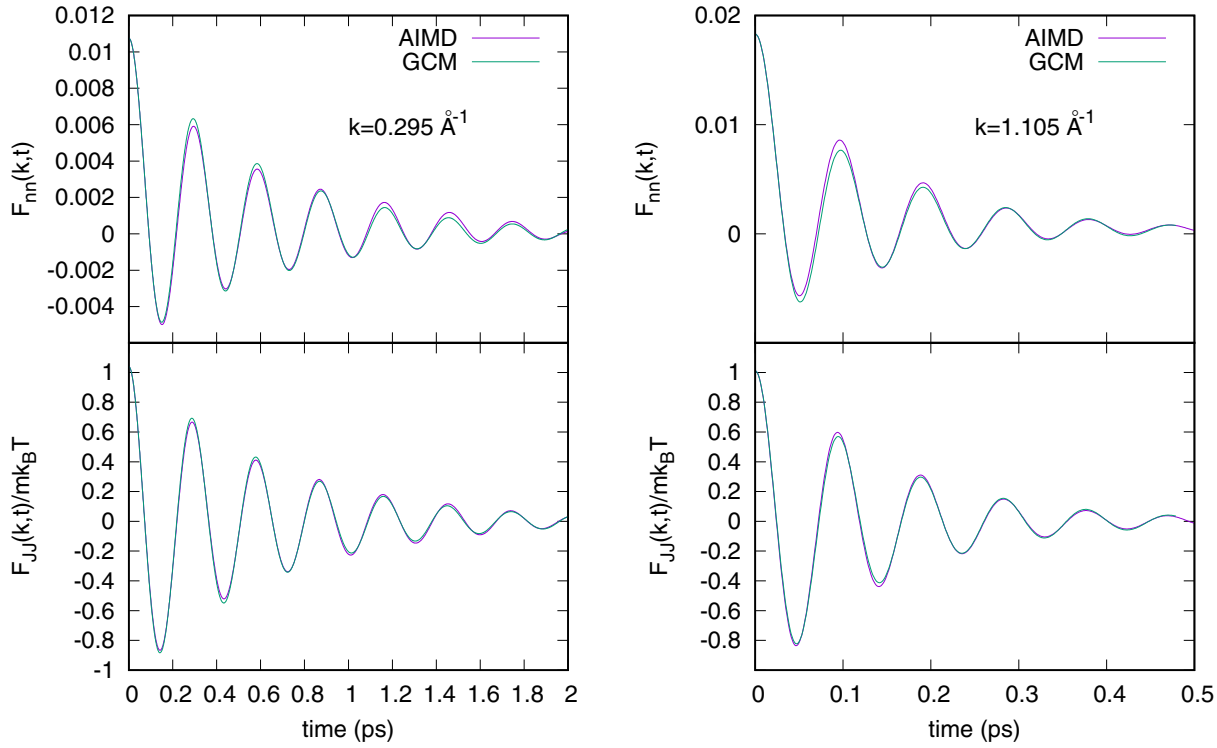


FIG. 15. Recovering of AIMD-derived density-density and longitudinal current-current time correlation functions by GCM theory for liquid iron at pressure 45 GPa and temperatures 2700 K in a wide range of wave numbers.

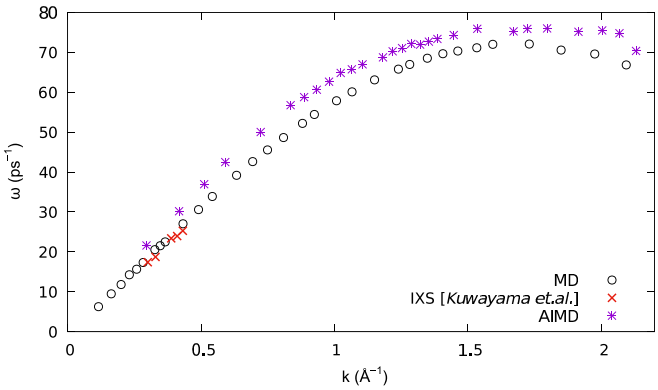


FIG. 16. Dispersion of collective excitations for liquid iron from EAM and *ab initio* simulations at pressure 45 GPa and temperatures 2700 K. Red cross symbols correspond to IXS experiments.

comparison with IXS experiments for liquid Fe at 2700 K [28]. To resolve this issue, one may try to use in AIMD more advanced exchange-correlation functionals, or to apply the Grimme D3 empirical dispersion corrections [62]. Namely, D3 dispersion corrections in the case of AIMD simulations of water [63] and an ice/water interface [64] allowed one to obtain a less rigid structure of water and improved the calculations of the ice melting temperature. Another, and perhaps more effective way to improve the dispersion of acoustic excitations, can account for spin polarization due to existing local magnetic moments. This would result in additional damping mechanisms of acoustic modes that should exist according to hydrodynamics of liquids with local magnetic moments.

(iii) We obtained among the dynamic eigenmodes of the thermoviscoelastic dynamic model the nonhydrodynamic heat waves, which are responsible for wavelike heat transfer at nanoscales in liquid Fe.

(iv) The detailed analysis of wave-number dependence of contributions to eigenvectors associated with acoustic modes allowed us to conclude that the mechanism of the "positive sound dispersion" is related with the increase of the contribution from diagonal stress tensor components to the sound eigenvalues, i.e., from instantaneous forces acting between particles, and which is absent in the long-wavelength limit implying that the macroscopic mechanism of sound propagation in liquids is solely due to the local conservation laws [65].

The future outlook for the analysis of collective dynamics in liquid Fe should be focused on accounting for local magnetic moments and spin-polarized electron density. For that purpose a combination of the spin-polarized AIMD simulations and a generalized hydrodynamic theory of metallic liquids with local magnetic moments should be developed. While the spin-polarized AIMD simulations of liquid Fe are a quite simple but time-consuming task, a theoretical scheme for analysis of AIMD-derived time correlation functions with explicit treatment of magnetic moments needs to be developed. One cannot directly use the spin-polarized electron densities in generalized hydrodynamics because in adiabatic approximation, which is used in almost all AIMD simulations, the true dynamics of electrons is neglected. However, it is possible within the DFT to derive an adiabatic dynamics of local magnetic moments as was suggested in [66]. Using this methodology one may explicitly calculate from AIMD simulations the time dependence of local magnetic moments and corresponding time correlation functions which can be along with density-density and other hydrodynamic time correlation functions analyzed by an extension of the scheme proposed by Mryglod, Folk, and co-workers [49–51]. Such a combination of AIMD simulations and generalized hydrodynamics of magnetic liquids would allow one to study the effect of magnetic moments on sound propagation and transport coefficients in liquid iron.

ACKNOWLEDGMENTS

T.B. was supported by the National Research Foundation of Ukraine Project No. 2023.05/0019. T.D. was supported by Project No. 09/01-2024 from the National Academy of Sciences of Ukraine for Youth Groups. The computations were enabled by resources provided by the National Academic Infrastructure for Supercomputing in Sweden (NAISS), partially funded by the Swedish Research Council through Grant Agreement No. 2022-06725. Support of the staff of the National Supercomputing Center (Linköping) is appreciated. A.B.B. acknowledges financial support from Nanjing University.

DATA AVAILABILITY

There are no publicly available research data or software supporting this manuscript. Requests for further information or data should be sent to the authors.

[1] Y. Sun, M. Mendelev, F. Zhang, X. Liu, B. Da, C.-Zh Wang, and R. M. Wentzcovitch, Unveiling the effect of Ni on the formation and structure of Earth's inner core, Proc. Natl. Acad. Sci. USA **121**, e2316477121 (2024).

[2] T. Liu and Z. Jing, Hydrogen and silicon are the preferred light elements in Earth's core, Commun. Earth. Environ. **5**, 282 (2024).

[3] A. J. Wilson, D. Alfe, A. M. Walker, and C. J. Davies, Can homogeneous nucleation resolve the inner core nucleation paradox? Earth Planet. Sci. Lett. **614**, 118176 (2023).

[4] X. Ma and H. Tkalcic, Seismic low-velocity equatorial torus in the Earth's outer core: Evidence from the late–coda correlation wavefield, Sci. Adv. **10**, eadn5562 (2024).

[5] P. M. Nasch, M. H. Manghnani, and R. A. Secco, Sound velocity measurements in liquid iron by ultrasonic interferometry, J. Geophys. Res. **99**, 4285 (1994).

[6] M. D. Rutter, R. A. Secco, H. Liu, T. Uchida, M. L. Rivers, S. R. Sutton, and Y. Wang, Viscosity of liquid Fe at high pressure, Phys. Rev. B **66**, 060102(R) (2002).

[7] R. A. Secco, M. D. Rutter, S. P. Balog, H. Liu, D. C. Rubie, T. Uchida, D. Frost, Y. Wang, M. Rivers, and S. R. Sutton, Viscosity and density of Fe–S liquids at high pressures, J. Phys.: Condens. Matter **14**, 11325 (2002).

[8] G. Shen, V. B. Prakapenka, M. L. Rivers, and S. R. Sutton, Structure of liquid iron at pressures up to 58 GPa, Phys. Rev. Lett. **92**, 185701 (2004).

[9] S. Hosokawa, M. Inui, K. Matsuda, D. Ishikawa, and Alfred Q. R. Baron, Damping of the collective modes in liquid Fe, Phys. Rev. B **77**, 174203 (2008).

[10] S. Hosokawa, M. Inui, K. Matsuda, D. Ishikawa, and A. Q. R. Baron, Collective dynamics of liquid Fe, J. Phys.: Conf. Ser. **98**, 022004 (2008).

[11] G. A. de Wijs, G. Kresse, L. Vocadlo, D. Dobson, D. Alfe, M. J. Gillan, and G. D. Price, The viscosity of liquid iron at the physical conditions of the Earth's core, Nature (London) **392**, 805 (1998).

[12] D. Alfe, M. J. Gillan, and G. D. Price, The melting curve of iron at the pressures of the Earth's core from *ab initio* calculations, Nature (London) **401**, 462 (1999).

[13] D. Alfe, G. Kresse, and M. J. Gillan, Structure and dynamics of liquid iron under Earth's core conditions, Phys. Rev. B **61**, 132 (2000).

[14] A. B. Belonoshko, R. Ahuja, and B. Johansson, Quasi–*ab initio* molecular dynamic study of Fe melting, Phys. Rev. Lett. **84**, 3638 (2000).

[15] H. K. Mao, J. Xu, V. V. Struzhkin, J. Shu, R. J. Hemley, W. Sturhahn, M. Y. Hu, E. E. Alp, L. Vocadlo, D. Alfe, G. D. Price, M. J. Gillan, M. Schwoerer-Böhning, D. Häusermann, P. Eng, G. Shen, H. Giefers, R. Lübbers, and G. Wortmann, Phonon density of states of iron up to 153 gigapascals, Science **292**, 914 (2001).

[16] L. Koči, A. B. Belonoshko, and R. Ahuja, Molecular dynamics study of liquid iron under high pressure and high temperature, Phys. Rev. B **73**, 224113 (2006).

[17] C. Desgranges and J. Delhommelle, Viscosity of liquid iron under high pressure and high temperature: Equilibrium and nonequilibrium molecular dynamics simulation studies, Phys. Rev. B **76**, 172102 (2007).

[18] W. Luo, B. Johansson, O. Eriksson, S. Arapan, P. Souvatzis, M. I. Katznelson, and R. Ahuja, Dynamical stability of body center cubic iron at the Earth's core conditions, Proc. Natl. Acad. Sci. USA **107**, 9962 (2010).

[19] A. B. Belonoshko, T. Bryk, and A. Rosengren, Shear relaxation in iron under the conditions of Earth's inner core, Phys. Rev. Lett. **104**, 245703 (2010).

[20] A. B. Belonoshko, S. Arapan, and A. Rosengren, An *ab initio* molecular dynamics study of iron phases at high pressure and temperature, J. Phys.: Condens. Matter **23**, 485402 (2011).

[21] A. B. Belonoshko, N. V. Skorodumova, S. Davis, A. N. Osiptsov, A. Rosengren, and B. Johansson, Origin of the low rigidity of the Earth's inner core, Science **316**, 1603 (2007).

[22] A. B. Belonoshko, N. V. Skorodumova, A. Rosengren, and B. Johansson, Elastic anisotropy of Earth's inner core, Science **319**, 797 (2008).

[23] A. B. Belonoshko, Equation of state for ε-iron at high pressures and temperatures, Condens. Matter Phys. **13**, 23605 (2010).

[24] T. Bryk and A. B. Belonoshko, Collective excitations in molten iron above the melting point: A generalized collective-mode analysis of simulations with embedded-atom potentials, Phys. Rev. B **86**, 024202 (2012).

[25] M. Marques, L. E. Gonzalez, and D. J. Gonzalez, *Ab initio* study of the structure and dynamics of bulk liquid Fe, Phys. Rev. B **92**, 134203 (2015).

[26] M. Marques, L. E. Gonzalez, and D. J. Gonzalez, Pressure-induced changes in structural and dynamic properties of liquid Fe close to the melting line. An *ab initio* study, J. Phys.: Condens. Matter **28**, 075101 (2016).

[27] L. E. Gonzalez and D. J. Gonzalez, Structure and dynamics in liquid iron at high pressure and temperature. A first principles study, J. Geophys. Res.: Solid Earth **128**, e2022JB025119 (2023).

[28] Y. Kuwayama, G. Morard, Y. Nakajima, K. Hirose, Alfred Q. R. Baron, S. I. Kawaguchi, T. Tsuchiya, D. Ishikawa, N. Hirao, and Y. Ohishi, Equation of state of liquid iron under extreme conditions, Phys. Rev. Lett. **124**, 165701 (2020).

[29] M. I. Mendelev, S. Han, D. J. Srolovitz, G. J. Ackland, D. Y. Sun, and M. Asta, Development of new interatomic potentials appropriate for crystalline and liquid iron, Philos. Mag. **83**, 3977 (2003).

[30] M. Pozzo, C. Davies, D. Gubbins, and D. Alfe, Thermal and electrical conductivity of iron at Earth's core conditions, Nature (London) **485**, 355 (2012).

[31] D. Alfe, G. D. Price, and M. J. Gillan, Iron under Earth's core conditions: Liquid-state thermodynamics and high-pressure melting curve from *ab initio* calculations, Phys. Rev. B **65**, 165118 (2002).

[32] P. Söderlind, J. A. Moriarty, and J. M. Wills, First-principles theory of iron up to Earth-core pressures: Structural, vibrational, and elastic properties, Phys. Rev. B **53**, 14063 (1996).

[33] E. G. Moroni, G. Kresse, J. Hafner, and J. Furthmüller, Ultrasoft pseudopotentials applied to magnetic Fe, Co, and Ni: From atoms to solids, Phys. Rev. B **56**, 15629 (1997).

[34] P. Ganesh and M. Widom, *Ab initio* simulations of geometrical frustration in supercooled liquid Fe and Fe-based metallic glass, Phys. Rev. B **77**, 014205 (2008).

[35] J.-P. Boon and S. Yip, *Molecular Hydrodynamics* (McGraw-Hill, New York, 1980).

[36] J.-P. Hansen and I. R. McDonald, *Theory of Simple Liquids* (Academic, London, 1986).

[37] T. Scopigno, G. Ruocco, and F. Sette, Microscopic dynamics in liquid metals: The experimental point of view, Rev. Mod. Phys. **77**, 881 (2005).

[38] T. Scopigno, U. Balucani, G. Ruocco, and F. Sette, Density fluctuations in molten lithium: Inelastic x-ray scattering study, J. Phys.: Condens. Matter **12**, 8009 (2000).

[39] T. Scopigno, G. Ruocco, F. Sette, and G. Viliani, Evidence of short-time dynamical correlations in simple liquids, Phys. Rev. E **66**, 031205 (2002).

[40] T. Scopigno, A. Filipponi, M. Krisch, G. Monaco, G. Ruocco, and F. Sette, High-frequency acoustic modes in liquid gallium at the melting point, Phys. Rev. Lett. **89**, 255506 (2002).

[41] D. J. Gonzalez, L. E. Gonzalez, J. M. Lopez, and M. J. Stott, Microscopic dynamics in the liquid Li-Na alloy: An *ab initio* molecular dynamics study, Phys. Rev. E **69**, 031205 (2004).

[42] D. J. Gonzalez, L. E. Gonzalez, J. M. Lopez, and M. J. Stott, Collective modes in liquid binary alloys. An *ab initio* molecular

dynamics study of the LiMg and LiBa alloys, J. Phys.: Condens. Matter **17**, 1429 (2005).

[43] W. Schirmacher and H. Sinn, Collective dynamics of simple liquids: A mode-coupling description, Condens. Matter Phys. **11**, 127 (2008).

[44] B. Schmid and W. Schirmacher, Modified mode-coupling theory for the collective dynamics of simple liquids, J. Phys.: Condens. Matter **23**, 254211 (2011).

[45] I. M. Mryglod, I. P. Omelyan, and M. V. Tokarchuk, Generalized collective modes for the Lennard-Jones fluid, Mol. Phys. **84**, 235 (1995).

[46] T. Bryk, Non-hydrodynamic collective modes in liquid metals and alloys, Eur. Phys. J.: Spec. Top. **196**, 65 (2011).

[47] T. Bryk, I. Mryglod, T. Scopigno, G. Ruocco, F. Gorelli, and M. Santoro, Collective excitations in supercritical fluids: Analytical and molecular dynamics study of "positive" and "negative" dispersion, J. Chem. Phys. **133**, 024502 (2010).

[48] T. Bryk, G. Ruocco, and A. P. Seitsonen, Stress fluctuations and adiabatic speed of sound in liquids: A simple way to estimate it from *ab initio* simulations, Sci. Rep. **13**, 18042 (2023).

[49] I. M Mrygold, I. M. Mryglod, and M. V. Tokarchuk, On the hydrodynamic theory of a magnetic liquid I. General description, Physica A **220**, 325 (1995).

[50] I. M. Mryglod and R. Folk, On the hydrodynamic theory of a magnetic liquid II. Hydrodynamic modes in the Heisenberg fluid, Physica A **234**, 129 (1996).

[51] I. Mryglod, R. Folk, S. Dubyk, and Y. Rudavskii, Hydrodynamic time-correlation functions of a Heisenberg ferrofluid, Physica A **277**, 389 (2000).

[52] P. E. Blöchl, Projector augmented-wave method, Phys. Rev. B **50**, 17953 (1994).

[53] G. Kresse and D. Joubert, From ultrasoft pseudopotentials to the projector augmented-wave method, Phys. Rev. B **59**, 1758 (1999).

[54] J. P. Perdew, K. Burke, and M. Ernzerhof, Generalized gradient approximation made simple, Phys. Rev. Lett. **77**, 3865 (1996).

[55] I. M. de Schepper, E. G. D. Cohen, C. Bruin, J. C. van Rijs, W. Montfrooij, and L. A. de Graaf, Hydrodynamic time correlation functions for a Lennard-Jones fluid, Phys. Rev. A **38**, 271 (1988).

[56] T. Bryk and G. Ruocco, Generalised hydrodynamic description of the time correlation functions of liquid metals: *Ab initio* molecular dynamics study, Mol. Phys. **111**, 3457 (2013).

[57] I. Tamblyn, J.-Y. Raty, and S. A. Bonev, Tetrahedral clustering in molten lithium under pressure, Phys. Rev. Lett. **101**, 075703 (2008).

[58] T. Bryk, S. De Panfilis, F. A. Gorelli, E. Gregoryanz, M. Krisch, G. Ruocco, M. Santoro, T. Scopigno, and A. P. Seitsonen, Dynamical crossover at the liquid-liquid transformation of a compressed molten alkali metal, Phys. Rev. Lett. **111**, 077801 (2013).

[59] L. Van Hove, Correlations in space and time and Born approximation scattering in systems of interacting particles, Phys. Rev. **95**, 249 (1954).

[60] C. W. Ryu and T. Egami, Alpha-relaxation by scattering and medium-range atomic correlation in simple liquids, J. Chem. Phys. **163**, 144506 (2025).

[61] T. Bryk, M. Kopcha, and G. Ruocco, *Ab initio* study of collective eigenmodes in dynamics of molten salts, J. Mol. Liq. **387**, 122622 (2023).

[62] S. Grimme, J. Antony, S. Ehrlich, and H. Krieg, A consistent and accurate *ab initio* parametrization of density functional dispersion correction (DFT-D) for the 94 elements H-Pu, J. Chem. Phys. **132**, 154104 (2010).

[63] T. Bryk and A. P. Seitsonen, *Ab initio* molecular dynamics study of collective excitations in liquid HO and DO: Effect of dispersion corrections, Condens. Matter Phys. **19**, 23604 (2016).

[64] A. P. Seitsonen and T. Bryk, Melting temperature of water: DFT-based molecular dynamics simulations with D3 dispersion correction, Phys. Rev. B **94**, 184111 (2016).

[65] T. Bryk, W. Schirmacher, and G. Ruocco, Comment on "deformations, relaxation and broken symmetries in liquids, solids and glasses: A unified topological field theory", Phys. Rev. E **106**, 036601 (2022).

[66] Q. Niu, X. Wang, L. Kleinman, W.-M. Liu, D. M. C. Nicholson, and G. M. Stocks, Adiabatic dynamics of local spin moments in itinerant magnets, Phys. Rev. Lett. **83**, 207 (1999).